JACS
JOURNAL OF THE AMERICAN CHEMICAL SOCIETY

ARTICLE

pubs.acs.org/JACS

Structure-Directing Roles and Interactions of Fluoride and Organocations with Siliceous Zeolite Frameworks

Ramzy M. Shayib,[†] Nathan C. George,[†] Ram Seshadri,[‡] Allen W. Burton,[§,#] Stacey I. Zones,[§] and Bradley F. Chmelka*[,†]

[†]Department of Chemical Engineering and [‡]Materials Department, University of California, Santa Barbara, California 93106, United States

[§]Chevron Energy Technology Company, Richmond, California 94801, United States

Supporting Information

ABSTRACT: Interactions of fluoride anions and organocations with crystalline silicate frameworks are shown to depend subtly on the architectures of the organic species, which significantly influence the crystalline structures that result. One- and two-dimensional (2D) ^{1}H, ^{19}F, and ^{29}Si nuclear magnetic resonance (NMR) spectroscopy measurements establish distinct intermolecular interactions among F^- anions, imidazolium structure-directing agents (SDA^+), and crystalline silicate frameworks for as-synthesized siliceous zeolites ITW and MTT. Different types and positions of hydrophobic alkyl ligands on the imidazolium SDA^+ species under otherwise identical zeolite synthesis compositions and conditions lead to significantly different interactions between the F^- and SDA^+ ions and the respective silicate frameworks. For as-synthesized zeolite ITW, F^- anions are established to reside in the double-four-ring (D4R) cages and interact strongly and selectively with D4R silicate framework sites, as manifested by their strong ^{19}F—^{29}Si dipolar couplings. By comparison, for as-synthesized zeolite MTT, F^- anions reside within the 10-ring channels and interact relatively weakly with the silicate framework as ion pairs with the SDA^+ ions. Such differences manifest the importance of interactions between the imidazolium and F^- ions, which account for their structure-directing influences on the topologies of the resulting silicate frameworks. Furthermore, 2D ^{29}Si{^{29}Si} double-quantum NMR measurements establish ^{29}Si—O—^{29}Si site connectivities within the as-synthesized zeolites ITW and MTT that, in conjunction with synchrotron X-ray diffraction analyses, establish insights on complicated order and disorder within their framework structures.

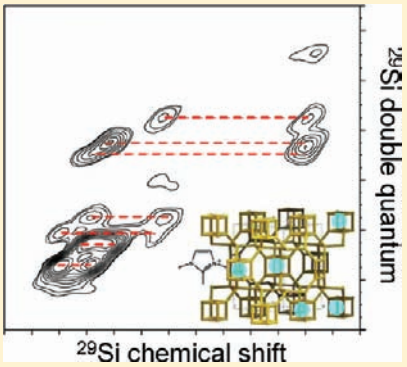

INTRODUCTION

The use of fluoride ions in zeolite syntheses has expanded the compositions, structures, and preparation conditions for diverse types of nanoporous crystalline silicate and aluminosilicate materials. This includes enabling the syntheses of siliceous zeolites with low defect densities or entirely new framework structures.[1−9] Nevertheless, despite the large influences that fluoride ions can have on zeolite crystallization, their interactions and roles in the formation of intricate framework structures remain poorly understood. This has been due to a combination of factors associated with multicomponent zeolite chemistry, the inherently nonequilibrium synthesis conditions, and the heterogeneities of the resulting products. Fluoride ions have previously been proposed to act as mineralizing agents and/or as catalysts for the formation of Si—O—Si bonds during gelation and/or crystallization.[10−12] On the other hand, the presence of F^- ions in as-synthesized zeolite materials, in some cases thought to interact strongly with zeolite frameworks,[13−15] has suggested structure-directing roles for fluoride, including the possibility that F^- anions stabilize small silicate rings and cages.[7,13,16−18] X-ray diffraction,[19−23] NMR spectroscopy,[13−15,24−26] and computational methods[17,27−29] have been used to assess the distributions of F^- anions in various siliceous zeolites, indicating different local environments. These include F^-—organocation ion pairs,[30] F^- anions in the centers of small cages that interact relatively weakly with framework atoms,[31] or as strongly interacting ligands to framework Si atoms forming five-coordinated SiO_4F^- moieties.[32,33] Little is known, however, about the specific molecular interactions among the F^- anions, SDA^+ molecules, and silicate frameworks that could account for distinct F^- anion distributions during zeolite syntheses, in the final as-synthesized crystalline products, or how they influence the framework topologies that result.

Zeolites ITW and MTT represent a particularly interesting pair of distinct structures that form as a result of crucially different interactions among F^- anions, SDA^+ molecules, and silicate framework moieties. Although they can be synthesized using similar alkyl-imidazolium SDAs under otherwise identical reaction conditions, zeolites ITW and MTT have frameworks with significantly different crystalline structures. As shown in Figure 1,

Received: June 12, 2011
Published: September 28, 2011

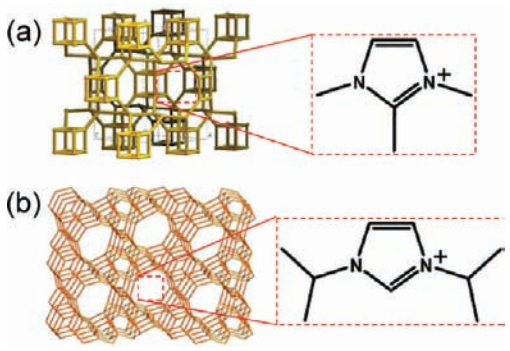

Figure 1. Schematic representations of (a) zeolite ITW and its corresponding structure-directing agent, *N*,*N*′-2-trimethylimidazolium, and (b) zeolite MTT and its corresponding SDA, *N*,*N*′-diisopropylimidazolium. Both zeolites were synthesized in otherwise identical fluoride-containing solutions, which, despite the similar SDA species, yield very different zeolite framework structures. F^- ions (not shown) are present in the as-synthesized materials to charge-balance the imidazolium organocations.

the ITW framework consists only of interconnected double-four-ring (D4R) cages, while the MTT framework consists of 10-ring channels and with no four-rings whatsoever. In such composite materials, the interactions and structure-directing roles of anionic F^- species have been difficult to establish. This has been due in part to possible disorder of the F^- anions associated with fully condensed and charge-neutral siliceous frameworks. Previous X-ray crystallography investigations[11,21,22] of as-synthesized zeolites ITW and MTT have indicated that, although the final zeolite frameworks exhibit long-range periodic order, the F^- ions and SDA^+ molecules appear not to retain similar degrees of positional registry,[14] making them challenging to observe by diffraction techniques.

By comparison, solid-state NMR spectroscopy is sensitive to the local (<1 nm) environments of ^1H, ^{19}F, and ^{29}Si species in both ordered and disordered materials. Furthermore, quantitative one-dimensional (1D) and correlative two-dimensional (2D) NMR methods can be used to identify and measure interactions between different $^{19}F^-$ anions or ^1H moieties of the cationic organic structure-directing molecules with framework ^{29}Si sites. Here, the locations and interactions of F^- and SDA^+ ions are established in as-synthesized siliceous zeolites ITW and MTT and are shown to account for their very different structural topologies that form under otherwise identical reaction compositions and conditions. The resulting molecular-level insights allow the significantly different structure-directing roles of F^- ions and their dependences on relatively subtle differences in the architectures of the SDA^+ molecules to be determined.

EXPERIMENTAL METHODS

Materials. Syntheses of the organocations *N*,*N*′-2-trimethylimidazolium and *N*,*N*′-diisopropylimidazolium (Figure 1) used as structure-directing agents (SDAs) to prepare fully siliceous forms of zeolite ITW and MTT have been previously described.[34] Imidazolium salts were initially prepared by alkylation of imidazole and subsequently ion-exchanged to form their respective hydroxide forms. The resulting SDAs were about 1 M in their corresponding aqueous solutions.

To increase the signal sensitivity of the NMR characterization measurements, all-silica ^{29}Si-enriched zeolites ITW and MTT were synthesized by adapting a previously reported synthesis procedure to

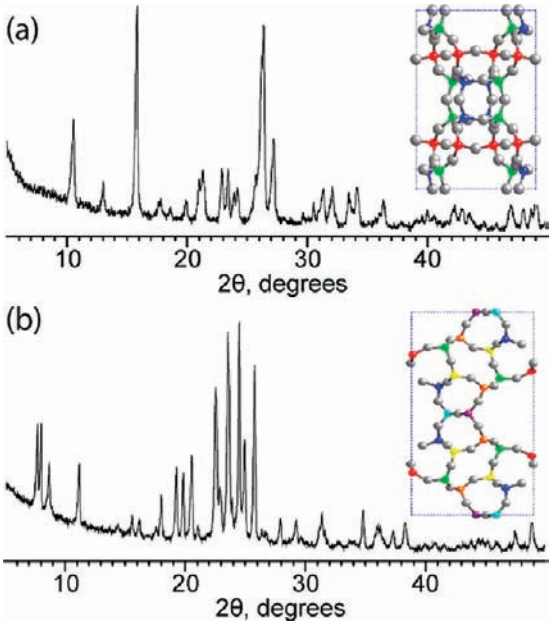

Figure 2. Powder X-ray diffraction patterns and previously reported unit cells for as-synthesized zeolites (a) ITW and (b) MTT.

include the use of $^{29}SiO_2$ (99% ^{29}Si basis) as the silica source. Reaction mixtures were prepared by using identical molar ratios of $1\ ^{29}SiO_2$: 0.5SDA (*N*,*N*′-2-trimethylimidazolium for zeolite ITW or *N*,*N*′-diisopropylimidazolium for zeolite MTT) in Teflon cups of Parr 4745 stainless-steel reactors, which were placed in a fume hood at room temperature for several days to evaporate the solution contents to near dryness. Water was then readded to each reaction mixture to obtain an H_2O/SiO_2 molar ratio of 14, and the mixtures were stirred for 5 min. Finally, appropriate amounts of 48−52 wt % HF (balance H_2O) were added to each mixture to achieve an HF/SDA molar ratio of 1 in the reaction mixtures. After being mixed for 1 min, tacky gels were obtained. The Parr reactors were then sealed and heated at 150 °C without mixing for 14 days. The resulting products were collected by vacuum filtration, washed in excess distilled H_2O, and air-dried at room temperature.

Characterization. The as-synthesized, siliceous, and ^{29}Si-enriched zeolite ITW and MTT products were characterized by powder X-ray diffraction and solid-state NMR spectroscopy. The long-range crystalline order of each product was established by wide-angle X-ray scattering. Powder X-ray diffraction (XRD) data were acquired using a Philips XPERT Pro diffractometer using Cu K_α radiation with λ = 1.5405 Å generated by a Philips high intensity ceramic sealed tube and a sealed proportional counter and X'celerator PSD detector. The samples were scanned at 3°/min between 2θ angles of 5−50°. For the as-synthesized products described above, the XRD patterns shown in Figure 2a,b are indexable to the ITW and MTT framework structures, respectively,[21,22,35,36] as established by fits of their simulated powder patterns. The absence of additional or broad XRD reflections (corresponding to superstructure or lower symmetry) in the two patterns establishes that no other crystalline or amorphous phases are present in the as-synthesized products, within the sensitivity of the XRD measurements. Previous powder XRD analyses[21] have placed the ITW structure under the space group *C*2/*m*, with three crystallographically distinct four-coordinate Si sites (so-called "tetrahedral", or "T-", sites), each occurring eight times per unit cell for a total of 24 T-sites in each ITW unit cell. An ITW unit cell with *C*2/*m* symmetry is shown in Figure 2a, with the blue, green, and red spheres representing the three crystallographically distinct T-sites in the ITW framework and the gray spheres representing bridging oxygen atoms. The blue and green T-sites occur in adjacent and alternating pairs that form cage-like double-four-ring (D4R) structures in the ITW framework

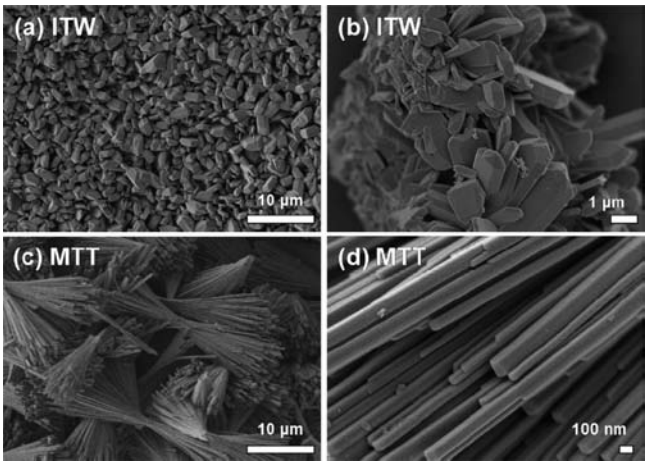

Figure 3. Scanning electron microscope (SEM) images of as-synthesized (a,b) zeolite ITW and (c,d) zeolite MTT.

and will henceforth be referred to as "D4R" sites, while the red T-sites connect two D4R cages and will be referred to as "D4R-bridging" sites. By comparison, single-crystal XRD analyses have established that the as-synthesized MTT structure falls under the space group $Pmn2_1$ and consists of seven crystallographically distinct T-sites.[22,37] Five of the T-sites occur four times per unit cell and the other two occur twice each, for a total of 24 T-sites per MTT unit cell, as shown in the inset of Figure 2b.

High-resolution synchrotron powder diffraction data were collected for as-synthesized and calcined zeolites ITW and MTT using the 11-BM beamline at the Advanced Photon Source (APS) at Argonne National Laboratory, using an average wavelength of 0.413167 Å. Details regarding data collection can be found elsewhere.[38−41] The unit cell parameters of all materials were found by indexing reflection positions with the software DICVOL06[42] and were further refined using a LeBail fit with the General Structure Analysis System (GSAS).[43,44] The structure of calcined ITW was refined by using the Rietveld method and GSAS, with energy minimizations conducted using the software Materials Studio. The MTT structures were refined starting from a model from previous single-crystal studies,[22] adjusting for unit cell parameters determined using DICVOL06. In the as-synthesized MTT structure, the positions of atoms that constitute the SDA^+ and F^- were not refined. Schematic diagrams of the structures were obtained using VESTA visualization software.[45] Refinements were completed by adjusting the profile shapes and unit cells during the LeBail fits, then refining the positions, and finally the atomic displacement parameters. When completed, all available structural parameters were allowed to refine simultaneously.

Scanning electron microscopy (SEM) images were collected using a Hitachi S-570 instrument. SEM images are shown in Figure 3 of as-synthesized zeolites ITW and MTT samples that were prepared using Cab-o-sil (SiO_2, 4.7% natural abundance ^{29}Si) under otherwise identical conditions as for the syntheses of the ^{29}Si-enriched zeolites ITW and MTT described above. The SEM images provide estimates of particle sizes and morphologies. For example, the SEM images in Figure 3a,b show as-synthesized zeolite ITW particles that are faceted polyhedra, approximately 2−3 μm in size. By comparison, Figure 3c,d shows SEM images of as-synthesized zeolite MTT particles that are in the form of bundles of long needle-like crystallites with individual lengths exceeding 20 μm and with widths as small as ∼100 nm.

Solid-state 1D and 2D nuclear magnetic resonance (NMR) spectroscopy measurements were conducted to characterize the molecular compositions and structures of the as-synthesized siliceous zeolites

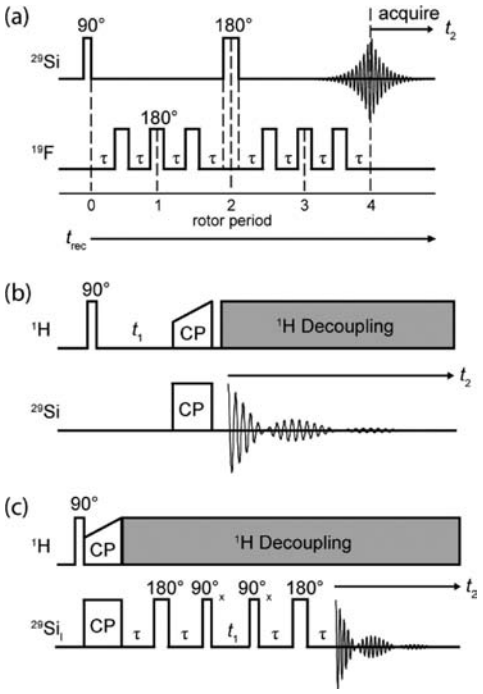

Figure 4. Schematic diagrams of solid-state NMR pulse sequences for (a) 1D $^{29}Si\{^{19}F\}$ rotational-echo double-resonance (REDOR), (b) 2D $^{29}Si\{^1H\}$ heteronuclear correlation (HETCOR), and (c) 2D refocused INADEQUATE (*J*-mediated) $^{29}Si\{^{29}Si\}$ double-quantum (DQ) NMR experiments.

ITW and MTT. Solid-state 1D single-pulse ^1H, ^{19}F, and ^{29}Si magic-angle-spinning (MAS) and $^{29}Si\{^{19}F\}$ rotational-echo double-resonance (REDOR) NMR experiments were conducted on a Bruker AVANCE NMR spectrometer with a 7.0 T wide-bore superconducting magnet, operating at frequencies of 300.1, 282.4, and 59.6 MHz corresponding to ^1H, ^{19}F, and ^{29}Si resonances, respectively. The measurements were performed under MAS conditions of 10 kHz for ^1H or 15 kHz for ^{19}F and ^{29}Si using a 2.5 mm variable-temperature H/F−X double-resonance MAS NMR probehead with zirconia rotors and Kel-F caps. Quantitative 1D single-pulse ^1H MAS experiments were performed using a 90° pulse length of 3.6 μs with a recycle delay of 1 s. Quantitative 1D single-pulse ^{19}F MAS experiments were conducted using a 90° pulse length of 2.3 μs with a recycle delay of 10 s for MTT and 60 s for ITW. Quantitative 1D single-pulse ^{29}Si MAS experiments were conducted using a 90° pulse length of 4.2 μs with a recycle delay of 300 s. The recycle delays were chosen to allow for complete spin relaxation of ^1H, ^{19}F, or ^{29}Si species (as determined by separate T_1 relaxation-time measurements) during signal averaging.

Interactions between different ^{29}Si framework sites and ^{19}F species within as-synthesized zeolites ITW and MTT were probed by using 1D $^{29}Si\{^{19}F\}$ REDOR NMR,[46] which is sensitive to the strengths of through-space $^{19}F-^{29}Si$ dipole−dipole couplings associated with nearby (∼1 nm) spin pairs. Rapid sample rotation at the magic angle (54.74°) generally averages anisotropic interactions, such as those associated with ^{29}Si and ^{19}F chemical shifts and dipolar couplings between nearby nuclei. However, by reintroducing $^{19}F-^{29}Si$ dipole−dipole couplings, the ^{29}Si signals of framework T-sites that interact with ^{19}F species are attenuated, according to the strengths of their heteronuclear couplings, which are proportional to $1/r^3$, where r is the distance separating two dipole−dipole-coupled nuclear spins, and which may be partially averaged by molecular motions. 1D $^{29}Si\{^{19}F\}$ REDOR spectra were acquired using two 4.75 μs ^{19}F 180° recoupling pulses per rotor

period,[46] a 300 s recycle delay, and different $^{19}F-^{29}Si$ dipolar recoupling times, t_{rec}, of 6.7 and 26.7 ms (100 and 400 rotor periods, respectively). 1D $^{29}Si\{^{19}F\}$ REDOR experiments were conducted without (S_0) and with (S) reintroduction of $^{29}Si-^{19}F$ dipolar couplings, the latter of which results in diminished ^{29}Si signal intensity that also takes into account effects from ^{29}Si T_1 relaxation that occurs during t_{rec}. A schematic diagram of the pulse sequence used to conduct the 1D $^{29}Si\{^{19}F\}$ REDOR experiments is shown in Figure 4a.

Specific molecular interactions between various ^{29}Si-framework and hydrogen-containing SDA moieties or $^{29}Si-O-^{29}Si$ site connectivities can be established by using solid-state 2D $^{29}Si\{^{1}H\}$ heteronuclear chemical shift correlation (HETCOR) or 2D J-mediated $^{29}Si\{^{29}Si\}$ double-quantum (DQ) NMR measurements, respectively.[47−53] 2D $^{29}Si\{^{1}H\}$ HETCOR NMR experiments rely on heteronuclear through-space $^{1}H-^{29}Si$ dipolar couplings, while 2D J-mediated $^{29}Si\{^{29}Si\}$ DQ NMR exploits homonuclear through-covalent-bond $^{29}Si-^{29}Si$ J (or synonymously "scalar") couplings. Although the couplings used by the two NMR techniques are intrinsically different, they both result in 2D spectra that represent frequency maps that allow interactions between specific molecular moieties to be correlated. The 2D $^{29}Si\{^{1}H\}$ HETCOR and J-mediated $^{29}Si\{^{29}Si\}$ DQ NMR experiments were conducted on a Bruker AVANCE III NMR spectrometer with an 18.8 T standard-bore superconducting magnet, operating at ^{1}H and ^{29}Si frequencies of 800.4 and 159.0 MHz, respectively. The measurements were performed under MAS conditions (8 kHz) using a 3.2 mm H−X−Y triple-resonance MAS NMR probehead with zirconia rotors and Kel-F caps. The 2D $^{29}Si\{^{1}H\}$ HETCOR experiments were conducted using a 3.2 μs ^{1}H 90° pulse, followed by an incremented evolution time t_1 prior to magnetization transfer to ^{29}Si nuclei using a 500 μs adiabatic cross-polarization pulse, and subsequently followed by ^{29}Si signal detection during the period t_2. For the short (500 μs) contact time used, correlated intensities arise predominantly from ^{29}Si and ^{1}H species separated by ca. 0.1−0.2 nm.[14] High-power broadband ^{1}H decoupling, using the pulse scheme small-phase-incremental-alternation-with-64-steps (SPINAL-64), was applied during ^{29}Si signal acquisition to enhance spectral resolution and sensitivity in the ^{29}Si dimension. A schematic diagram of the pulse sequence used for the 2D $^{29}Si\{^{1}H\}$ HETCOR experiments is shown in Figure 4b.

The 2D J-mediated $^{29}Si\{^{29}Si\}$ DQ NMR measurements were conducted using the refocused INADEQUATE technique,[50−52] which probes $^{29}Si-^{29}Si$ spin pairs that are scalar (J)-coupled through covalent bonds. The experiments used a 3.2 μs ^{1}H 90° pulse, followed by an 8 ms adiabatic cross-polarization pulse to transfer magnetization to ^{29}Si nuclei. A rotor-synchronized echo ($\tau-180°-\tau$) of total duration 2τ = 12 ms and with a 7.2 μs ^{29}Si 180° pulse was used to generate antiphase coherences under scalar (J_{Si-Si}) coupling evolution, while refocusing chemical shift interactions. The antiphase magnetization was converted by a 3.6 μs ^{29}Si 90° pulse into a mixture of double- and zero-quantum coherences, the latter of which were removed by phase-cycling and the former of which were detected indirectly by incrementation of the evolution period t_1. A subsequent ^{29}Si 90° pulse converted the remaining double-quantum components into antiphase coherences. After another delay τ, these were converted by a final 180° pulse into in-phase single-quantum coherences that evolved again under J_{Si-Si} interactions, forming an echo that initiated the detection period t_2. The value of τ = 6 ms was established to provide maximum signal intensity. Fourier transformation of the time-domain signals resulted in 2D refocused INADEQUATE $^{29}Si\{^{29}Si\}$ NMR spectra that represent frequency maps with single-quantum (SQ) and double-quantum (DQ) dimensions. Signals in the SQ dimension (horizontal axis) correspond to isotropic ^{29}Si chemical shifts, ω_i (similar to 1D ^{29}Si MAS spectra), while signals in the DQ dimension (vertical axis) represent the sum of the chemical shifts of two correlated J-coupled ^{29}Si nuclear spins, $\omega_i + \omega_j$. Pairs of signal intensities at (ω_i, $\omega_i + \omega_j$) and (ω_j, $\omega_i + \omega_j$) establish unambiguously that ^{29}Si species with SQ isotropic chemical shifts ω_i and ω_j are bonded covalently (in this case through bridging oxygen atoms). A schematic diagram of the pulse sequence used to conduct the 2D refocused INADEQUATE (J-mediated) $^{29}Si\{^{29}Si\}$ DQ experiments is shown in Figure 4c.

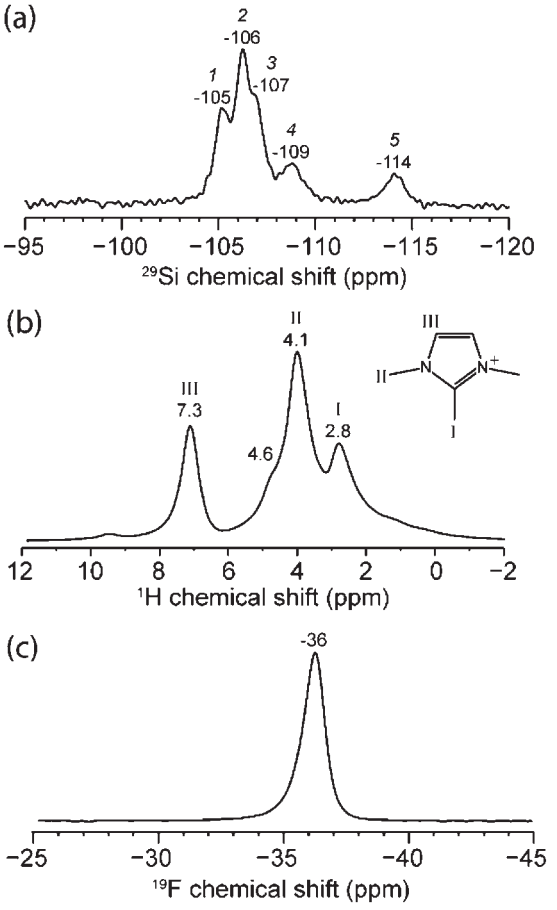

Figure 5. Solid-state 1D single-pulse (a) ^{29}Si, (b) ^{1}H, and (c) ^{19}F MAS NMR spectra of as-synthesized zeolite ITW acquired at room temperature under MAS conditions of 10 kHz for ^{1}H or 15 kHz for ^{19}F and ^{29}Si. Proton chemical shift assignments are shown in the inset in (b) for the structure-directing organocation *N,N′*-2-trimethylimidazolium.

RESULTS AND DISCUSSION

The locations and roles of the fluoride species, as well as the organocation structure-directing agents, have been difficult to elucidate because of their lower extents of order, as compared to the crystalline silicate frameworks. X-ray scattering analyses are sensitive to long-range atomic ordering and thus able to establish the structures of crystalline zeolite frameworks. However, scattering analyses are generally less suitable for components, such as the SDAs or fluoride species, that often have lower extents of periodic order. For as-synthesized zeolite ITW, the relatively large *N,N′*,2-trimethylimidazolium SDA^+ molecules are expected to reside within the large $[4^45^46^48^4]$ cages of the ITW framework formed by six interconnected D4R cages.[36] Similarly for as-synthesized zeolite MTT, the larger *N,N′*-diisopropylimidazolium SDA^+ molecules are presumed to be within the 10-ring channels of the MTT framework.[22] However, for both as-synthesized ITW and MTT materials, the absence of indexable

XRD reflections corresponding to the SDA^+ molecules indicates that the organocations do not exhibit high degrees of long-range atomic order with respect to their distributions and/or configurations within their respective cages or channels.

Despite the lack of long-range periodic order of the SDA^+ molecules, fluoride species appear to retain some long-range ordering in as-synthesized zeolites ITW and MTT. From powder and single-crystal XRD analyses, fluoride anions have been determined to reside within the D4R cages and five-ring cages of as-synthesized zeolites ITW and MTT, respectively.[21,22,36] However, unlike the SDA^+ molecules, the fluoride anions are sufficiently small to reside within any of the cages and/or channels of these zeolite frameworks. This can result in distributions of F^- anions among the different cages or channels, which, if disordered, cannot easily be distinguished nor ruled out on the basis of scattering techniques. Consequently, the distributions, mutual interactions, and structure-directing influences of the SDA^+ cations and the F^- anions with respect to their siliceous frameworks have remained elusive.

As-Synthesized Zeolite ITW. Although powder X-ray diffraction analyses have generally indicated three crystallographically distinct Si T-sites in the ITW structure, quantitative solid-state single-pulse ^{29}Si MAS NMR of as-synthesized zeolite ITW reveals at least five ^{29}Si framework species. As shown in Figure 5a, five incompletely resolved resonances are observed, centered at approximately −105, −106, −107, −109, and −114 ppm (labeled as "1", "2", "3", "4", and "5", respectively) with relative integrated signal intensities of approximately 1:2:1:1:1. On the basis of their chemical shifts, all five resonances are attributed to fully condensed Q^4 ^{29}Si species (where Q^4 represents four-coordinate Si atoms covalently bonded through bridging oxygen atoms to four other Si atoms).[54] By comparison, previous ^{29}Si MAS NMR measurements of calcined zeolite ITW also revealed signals from five Q^4 ^{29}Si species, however, with different chemical shifts ranging from ca. −109 to −118 ppm and different relative intensities, the assignments of which have remained unspecified (Figure S1a).[21] The similar numbers of ^{29}Si signals observed before and after calcination, both of which are larger than the three T-sites in the *C*2/*m* structure (Figure 2a), indicate that the symmetry of the framework may be lower than suggested by the scattering analyses. Contraction of the ITW framework and elimination of the organocation and fluoride species that occur upon calcination result in changes to local ^{29}Si environments that influence their isotropic chemical shifts.[53] On the basis of the XRD analyses of zeolite ITW before and after calcination (discussed in detail below), the changes in Si−O−Si bond angles or distances are relatively small, so that their influences are not expected to dominate. Rather, the appearance of the ^{29}Si resonances at generally lower shift values after calcination suggests that the local environments of the ^{29}Si framework species are influenced by their molecular interactions with the SDA^+ and/or F^- ions present in the as-synthesized material. Moreover, the relatively narrow (∼1 ppm, full-width-at-half-maximum, fwhm) ^{29}Si MAS lineshapes observed for the different framework sites in as-synthesized zeolite ITW reflect relatively high degrees of local site order. This establishes that ^{29}Si species occupying the same crystallographic sites experience similar interactions with the SDA^+ and/or F^- ions across the bulk sample.

By comparison, while the structure-directing *N*,*N*′-2-trimethylimidazolium species lack long-range positional registry in as-synthesized zeolite ITW, they nevertheless occupy relatively uniform local environments. This is determined from the single-pulse ^{1}H MAS NMR spectrum shown in Figure 5b of as-synthesized zeolite ITW, which exhibits three resolved ^{1}H signals centered at approximately 2.8, 4.1, and 7.3 ppm (labeled "I", "II", and "III", respectively). These are assigned to the three distinct ^{1}H moieties of *N*,*N*′-2-trimethylimidazolium: the methyl protons (I) at the 2 position of the imidazolium ring, methyl protons (II) at the *N* and *N*′ (i.e., 1 and 3) positions of the imidazolium ring, and ring protons (III) at the 4 and 5 positions of the imidazolium ring, respectively. (In addition, a partially resolved shoulder at ca.

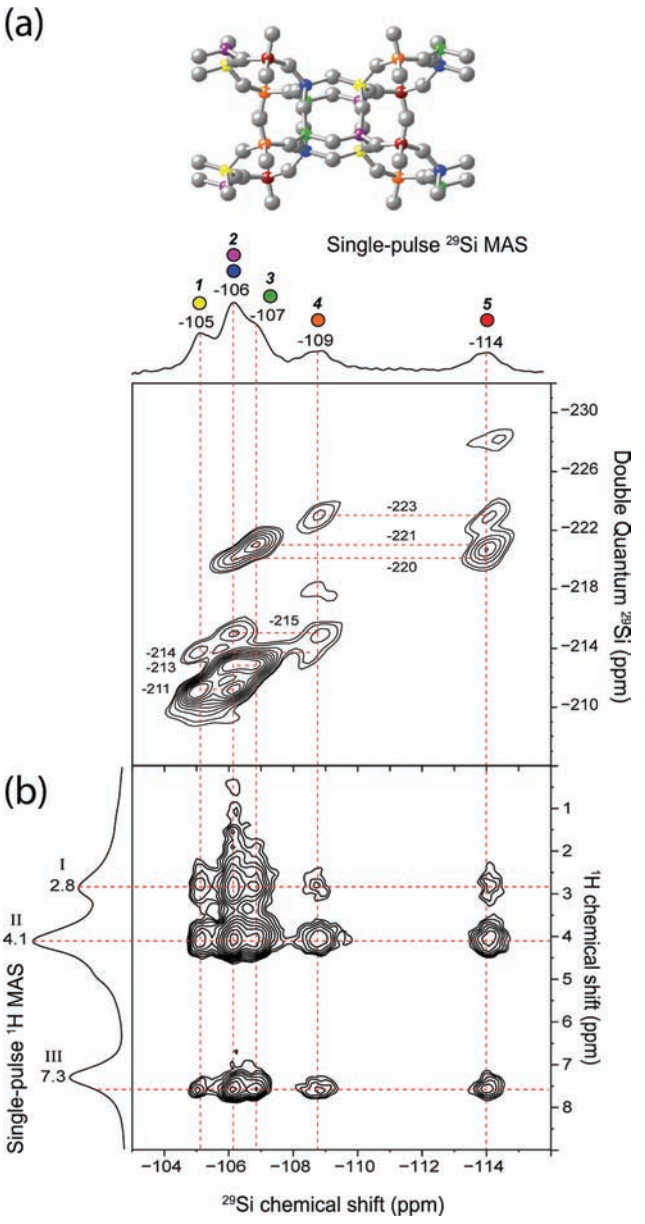

Figure 6. Solid-state (a) 2D refocused INADEQUATE (*J*-mediated) ^{29}Si{^{29}Si} double quantum (DQ) and (b) 2D ^{29}Si{^{1}H} heteronuclear correlation (HETCOR, dipolar-mediated) NMR spectra of as-synthesized zeolite ITW acquired at room temperature and 10 kHz MAS. Solid-state 1D single-pulse ^{29}Si and ^{1}H MAS NMR spectra are shown along the top horizontal and the left vertical axes, respectively, of the HETCOR spectrum. ^{29}Si chemical shift assignments are shown in (a) for the ITW structure (inset) with $P2_1$ space group symmetry.

4.6 ppm is observed that is attributed to adsorbed water.) The relatively narrow (~0.5 ppm fwhm) ^{1}H MAS lineshapes indicate that the SDA^{+} molecules occupy relatively uniform environments within as-synthesized zeolite ITW. Such uniformity is attributed in part to motions (translational or rotational) of the SDA^{+} molecules that are fast as compared to the time scale of the ^{1}H NMR measurement (~1 ms) and partially average otherwise large ^{1}H−^{1}H dipolar couplings. ^{1}H MAS NMR thus establishes that the SDA^{+} molecules occupy similar local environments, consistent with the SDA^{+} species residing in the large [$4^{4}5^{4}6^{4}8^{4}$] cages formed by the interconnected D4R cages of the ITW framework (Figure 1a).

Understanding the types, distributions, and local environments of fluoride anions within as-synthesized zeolite ITW is expected to provide important additional structure-directing insights on how the different types of cages form. Consistent with previous powder XRD analyses, the single-pulse ^{19}F MAS NMR spectrum in Figure 5c of as-synthesized zeolite ITW shows only a single narrow (~1 ppm fwhm) ^{19}F signal at ca. −36 ppm, indicating that all ^{19}F species are in similar local environments. ^{19}F NMR studies[9,24,31,55] previously conducted on diverse as-synthesized zeolites containing fluoride species have sought to correlate measured ^{19}F chemical shifts with where the F^{-} anions reside. Comparisons to such studies and complementary XRD investigations suggest that the resonance at −36 ppm is representative of F^{-} ions within the D4R cages of the ITW framework.[36] This indicates the F^{-} and SDA^{+} ions may occupy distinctly different types of cages in as-synthesized zeolite ITW, while remaining sufficiently near to maintain local charge neutrality.

While the types and relative populations of species can be established by single-pulse MAS NMR measurements, powerful double-resonance and/or multidimensional NMR techniques yield detailed insights on intermolecular interactions between the different components of as-synthesized zeolite ITW. In particular, techniques that rely on through-space dipolar couplings or through-bond *J* couplings can be used to determine local proximities and/or connectivities of two NMR-active nuclei. These include the ^{1}H, ^{19}F, and ^{29}Si species associated with the SDA^{+} molecules, F^{-} anions, and silicate framework species, respectively. For example, 2D *J*-mediated ^{29}Si{^{29}Si} DQ NMR experiments are sensitive to *J* couplings that allow ^{29}Si−O−^{29}Si site connectivities to be established.[47,48] Figure 6a shows a 2D *J*-mediated ^{29}Si{^{29}Si} DQ NMR spectrum of as-synthesized zeolite ITW that exhibits correlated single- and double-quantum signal intensities among all five ^{29}Si signals, allowing their interconnectivities within the ITW framework to be determined. Specifically, the single-quantum (SQ) signal at −105 ppm corresponding to ^{29}Si site "1" exhibits correlated signal intensities at −211 and −214 ppm in the DQ dimension, which establish that ^{29}Si site "1" is bonded covalently (through bridging oxygen atoms) to ^{29}Si sites "2" and "4", respectively. Similarly, the ^{29}Si signal at −106 ppm in the SQ dimension associated with ^{29}Si site "2" is correlated to signals at −211, −213, −215, and −220 ppm in the DQ dimension, which establish connectivities to ^{29}Si sites "1", "3", "4", and "5", respectively. The SQ signal at −107 ppm associated with ^{29}Si site "3" shows DQ intensity correlations at −213 and −221 ppm corresponding to ^{29}Si−O−^{29}Si bonds to ^{29}Si sites "2" and "5", respectively. Likewise, the ^{29}Si signal at −109 ppm in the SQ dimension attributed to ^{29}Si site "4" exhibits correlated signal intensities at −215, −218, and −223 ppm in the DQ dimension that establish covalent bonds to ^{29}Si site "1", another site "4", and site "5", respectively. Finally, the SQ signal at −114 ppm corresponding to ^{29}Si site "5" shows intensity correlations at −220, −221, −223, and −228 in the DQ dimension, establishing bonds to ^{29}Si sites "2", "3", "4", and another ^{29}Si site "5". Consequently, the 2D *J*-mediated ^{29}Si{^{29}Si} DQ NMR spectrum allows all of the ^{29}Si−O−^{29}Si connectivities among the distinct ^{29}Si framework sites in the zeolite ITW framework to be established. Furthermore, due to their interconnectivities, all of the ^{29}Si sites are unambiguously shown to be part of the same silicate framework structure, ruling out the presence of separate commingled frameworks with different topologies.

Along with identifying ^{29}Si−O−^{29}Si site connectivities, careful scrutiny of the correlated signal intensities of the 2D *J*-mediated ^{29}Si{^{29}Si} DQ NMR spectrum (Figure 6a) of as-synthesized zeolite ITW also yields insights on multiplicities of connectivities between otherwise identical ^{29}Si sites.[56] In particular, based solely on the ^{29}Si−O−^{29}Si connectivities identified in Figure 6a, the local environments of fully condensed Q^{4} ^{29}Si sites "1" and "3" remain incompletely specified, with only two of the four neighboring T-sites established: ^{29}Si site "1" is connected to sites "2" and "4", and ^{29}Si site "3" is bonded to sites "2" and "5". This suggests that ^{29}Si sites "1" and "3" have additional covalent connectivities to similar ^{29}Si sites. In fact, such connectivities to multiple similar framework moieties are clearly manifested in the relative intensities of the correlated signal pairs. For example, the pair of correlated ^{29}Si signals at (−105 SQ ppm, −211 DQ ppm) and (−106 SQ ppm, −211 DQ ppm), associated with covalent bonds between ^{29}Si sites "1" and "2", exhibits intensities that are approximately 3 times the magnitude of the correlated signal pair at (−105 SQ ppm, −214 DQ ppm) and (−109 SQ ppm, −214 DQ ppm), associated with covalent bonds between ^{29}Si sites "1" and "4". This indicates that ^{29}Si site "1" is bonded via bridging oxygen atoms to one site-"4" and to three site-"2" ^{29}Si atoms, fully specifying the four-coordinate local environment of the site-"1" moieties. Similarly, the correlated pair of ^{29}Si signals at (−106 SQ ppm, −213 DQ ppm) and (−107 SQ ppm, −213 DQ ppm), reflecting covalent bonds between ^{29}Si sites "2" and "3", exhibits intensities that are the same magnitude as those for the ^{29}Si signal pair associated with sites "1" and "2". Furthermore, these signals are 3 times as intense as those observed for the correlated pair of signals at (−107 SQ ppm, −221 DQ ppm) and (−114 SQ ppm, −221 DQ ppm) associated with ^{29}Si−O−^{29}Si connectivities between sites "3" and "5". Thus, each site "3" is established to similarly share ^{29}Si−O−^{29}Si bonds to one site-"5" and to three site-"2" ^{29}Si atoms, fully specifying the local four-coordinate environment of site "3" in the ITW framework.

While such connectivities fully specify the four neighboring T-sites of Q^{4} ^{29}Si sites "1" and "3", site "2" appears to be overspecified, with a total of eight connectivities (three to site "1", three to site "3", one to site "4", and one to site "5"). This indicates that Q^{4} ^{29}Si site "2" moieties are in fact comprised of two crystallographically distinct framework sites with nearly identical isotropic ^{29}Si chemical shifts. Such convolution of overlapping ^{29}Si signals associated with two different framework sites ("2a" and "2b") is supported by the quantitative single-pulse ^{29}Si MAS spectrum in Figure 5a, in which their overlapping ^{29}Si signals at −106 ppm exhibit integrated intensity that is twice that of each of the other signals at −105, −107, −109, and −114 ppm corresponding to ^{29}Si sites "1", "3", "4", and "5", respectively. On the basis of the ^{29}Si−O−^{29}Si site connectivities

established by 2D *J*-mediated $^{29}Si\{^{29}Si\}$ DQ NMR, in conjunction with powder XRD analyses, ^{29}Si framework sites "1", "2a", "2b", and "3" are concluded to be part of the D4R cages (Figure 6 inset, yellow, blue, purple, green spheres), while ^{29}Si sites "4" and "5" correspond to bridging moieties between different D4R cages (Figure 6 inset, orange red spheres). This is corroborated by quantitative single-pulse ^{29}Si MAS measurements that yield combined integrated signal intensities for ^{29}Si sites "1", "2a", "2b", and "3" that account for 2/3 of all ^{29}Si species, as compared to 1/3 for ^{29}Si sites "4" and "5", which agree with the expected ratio of D4R to D4R-bridging T-sites in the ITW unit cell. Thus, the interconnectivities are unambiguously established, although the six distinct framework T-sites in the as-synthesized zeolite ITW structure cannot be reconciled to the *C*2/*m* space group suggested by prior powder XRD analyses.

On the basis of the $^{29}Si-O-^{29}Si$ connectivities and populations established by these detailed 1D and 2D NMR analyses, the as-synthesized zeolite ITW framework is determined to have lower symmetry than the *C*2/*m* space group classification. Yang et al.[36] previously proposed a lower symmetry space group to account for the greater number of distinct ^{29}Si sites observed in ^{29}Si MAS NMR spectra of calcined zeolite ITW. On the basis of Rietveld refinement analyses of synchrotron X-ray diffraction data and energy minimization calculations, they suggested the *Cm* space group for the structure of as-synthesized zeolite ITW. However, the *Cm* space group also cannot be reconciled with all of the NMR data, specifically the interconnectivities among the different T-sites. While the *Cm* structure contains six crystallographically distinct T-sites and is thus consistent with the 1D ^{29}Si MAS NMR spectrum (Figure 5a), it would manifest covalent bonds (via bridging oxygen atoms) between two identical ^{29}Si T-sites within the D4R cages, which does not agree with $^{29}Si-O-^{29}Si$ connectivities established by the 2D *J*-mediated $^{29}Si\{^{29}Si\}$ DQ spectrum in Figure 6a. The *J*-mediated $^{29}Si\{^{29}Si\}$ DQ results provide sensitive information and important structural constraints on the molecular connectivities and short-range ordering in as-synthesized zeolite ITW, which point to a structure with lower symmetry than previously proposed.

On the basis of the structural constraints and symmetry insights obtained from the 2D ^{29}Si NMR analyses above, synchrotron X-ray diffraction data were collected and analyzed to distinguish among framework structural models with different long-range atomic periodicities. Synchrotron scattering techniques result in diffraction patterns with significantly higher sensitivity and resolution than conventional (Cu K_α) powder XRD methods, which allow much more detailed and accurate structural analyses. For example, Figure 7a,b shows synchrotron powder XRD data for as-synthesized and calcined zeolite ITW, which are compared to calculated patterns for candidate structures with *C*2 and $P2_1/m$ space-group symmetries. In particular, comparison of the synchrotron data to the pattern calculated using the *C*2 space group shows significant differences between the two. Specifically, the *C*2 structural model does not account for the reflections near 2.4° and 4.9° 2θ, in addition to other small reflections at larger 2θ values. (Previously proposed *C*2/*m* and *Cm* structural models yielded much worse fits.) The reflections near 2.4° and 4.9° 2θ are, however, accounted for by the $P2_1/m$ space group. Moreover, the reflection near 2.1° 2θ can only be modeled by doubling the *c*-axis of the conventional ITW unit cell from 8.85 to 17.7 Å, which also doubles the number of crystallographically distinct T-sites from 6 to 12, although the slight differences in their local environments are not resolved by

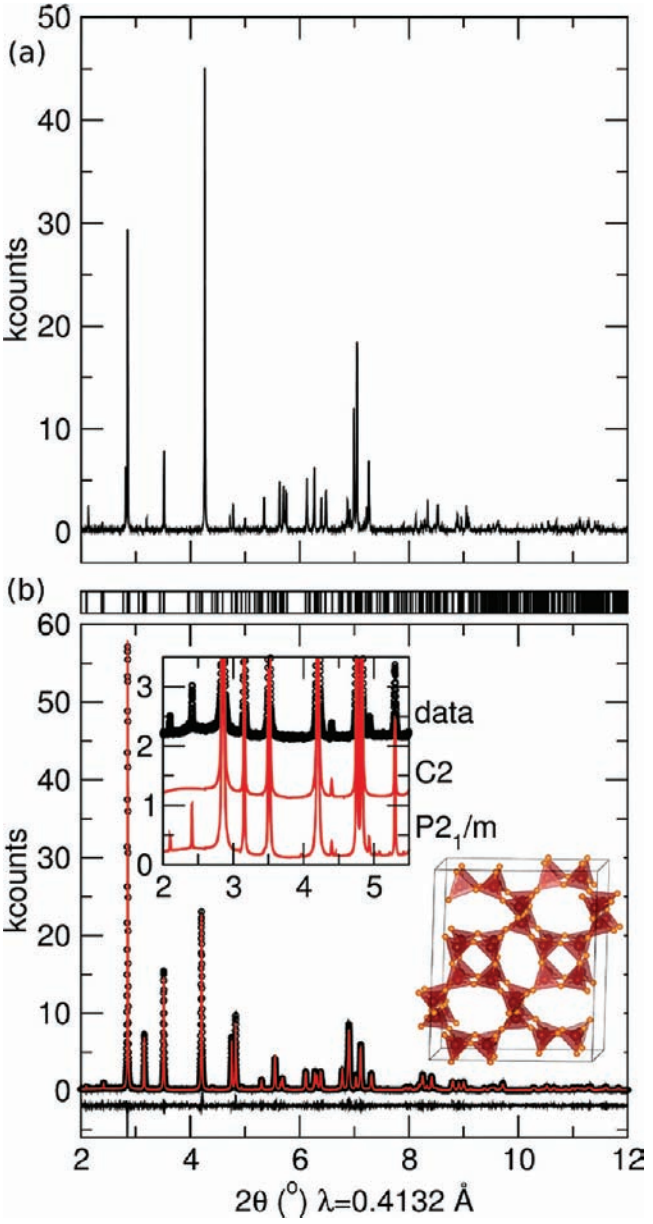

Figure 7. Synchrotron X-ray powder diffraction pattern of (a) as-synthesized and (b) calcined zeolite ITW. The solid red lines correspond to the Rietveld fits performed using the $P2_1/m$ space group; the open circles correspond to experimental data, and the solid black lines represent the difference between simulated and experimental data. Expected reflection positions are shown on the top of (b). The inset in (b) is a magnification of the 2θ range 2−5.5° comparing Rietveld fits performed using the *C*2 (single *c*-axis) or $P2_1/m$ (doubled *c*-axis) space groups with the experimental data. A schematic diagram of the refined calcined zeolite ITW structure looking down the *a*-axis is shown in (b), with Si atoms at the center of each tetrahedron and oxygen atoms depicted as orange.

solid-state ^{29}Si NMR.[21] The Rietveld refinement of the calcined zeolite ITW in Figure 7b shows the excellent fit obtained by using the $P2_1/m$ structural model (χ^2 = 1.645). A list of the structural and atomic parameters can be found in the Supporting Information, Table S1. The siliceous framework structure of calcined zeolite ITW is thus confidently determined to exhibit $P2_1/m$ symmetry.

For as-synthesized zeolite ITW, however, framework interactions with the structure-directing organocations and fluoride anions reduce the symmetry of the overall structure. This is evident both in the additional distinct Si T-sites resolved by ^{29}Si NMR (Figures 5 and 6) and by the fact that the strong reflection near 2.9° 2θ is approximately one-half the intensity for as-synthesized zeolite ITW as compared to the calcined material (Figure 7), indicating less coherent long-range periodicity of the (110) plane. Closer scrutiny of the $P2_1/m$ model that well-describes the structure of calcined zeolite ITW clearly establishes that crystallographically equivalent Si T-sites in the D4R cages are covalently bonded to each other through a bridging oxygen atom. However, the 2D ^{29}Si NMR results (Figure 6) for as-synthesized zeolite ITW clearly establish that T-sites in the D4R cages are not covalently bonded to each other. To reconcile this, the mirror plane in the $P2_1/m$ structure must be removed, resulting in a lower symmetry space group for as-synthesized zeolite ITW. A structural model based on the lower symmetry $P2_1$ space group allows all of the positions of even the lowest-intensity synchrotron XRD reflections to be matched and is furthermore consistent with the Si T-site interconnectivities established by 2D ^{29}Si NMR. It should be noted that matching the intensities of the synchrotron XRD reflections is challenging, due to the inherent disorder of the SDA$^+$ and F$^-$ distributions in the as-synthesized material. Reflection positions and intensities change considerably upon calcination of zeolite ITW (Figure 7a,b), manifesting the differences in symmetry and resulting unit cell parameters (Supporting Information, Table S2). Such changes indicate that framework interactions with the structure-directing agents strongly influence the symmetry of the crystallographic structure of zeolite ITW. The combination of 2D ^{29}Si NMR and synchrotron XRD analyses thus provides complementary and detailed information on short- and long-range structural ordering, consistent with $P2_1$ symmetry of as-synthesized zeolite ITW.

The symmetry of the ITW structure and how it develops arises from complicated interactions among the crystallizing silicate framework, organocation SDA$^+$ species, and fluoride anions. Whereas through-bond ^{29}Si J couplings are used to establish connectivities among the silicate framework sites, through-space dipolar interactions provide insights on molecularly proximate species (<1 nm) that do not necessarily share covalent bonds. In particular, interactions between hydrogen-containing moieties of the SDA$^+$ molecules and the various ^{29}Si framework moieties in as-synthesized ITW are directly and unambiguously established by 2D ^{29}Si{^{1}H} HETCOR NMR measurements (Figure 4b) that correlate the isotropic ^{29}Si and ^{1}H chemical shifts of ^{29}Si—^{1}H dipole—dipole-coupled moieties. For example, Figure 6b shows a 2D ^{29}Si{^{1}H} HETCOR NMR spectrum of as-synthesized ITW that exhibits correlated signal intensities between all of the ^{29}Si signals associated with the silicate framework sites of as-synthesized zeolite ITW and the various ^{1}H signals associated with the *N*,*N*′-2-trimethylimidazolium SDA$^+$ molecules. Specifically, intensity correlations are clearly visible between each of the three ^{1}H signals (at 2.8, 4.1, and 7.3 ppm in the ^{1}H dimension) associated with the distinct moieties I, II, and III of the SDA$^+$ molecule and each of the five resolved ^{29}Si resonances (at −105, −106, −107, −109, and −114 ppm in the ^{29}Si dimension) from T-sites in the ITW framework. Furthermore, the correlated signal intensities are approximately proportional to the relative populations of their associated ^{29}Si sites and ^{1}H species, indicating that each ^{1}H-containing moiety of the *N*,*N*′-2-trimethylimidazolium SDA$^+$ molecules interacts nonselectively and similarly with all of the different ^{29}Si framework sites. As the strengths of dipole—dipole interactions depend on molecular separation distances and mobilities, the 2D ^{29}Si{^{1}H} HETCOR spectrum in Figure 6b of as-synthesized zeolite ITW is consistent with the SDA$^+$ molecules occupying the [$4^4$$5^4$$6^4$$8^4$] cages of the ITW framework. In such environments, the SDA$^+$ molecules can interact with the different framework T-sites, while retaining relatively high mobilities (relative to the 1 ms time scale of the NMR measurement), consistent with the relatively narrow lineshapes revealed by single-pulse ^{1}H MAS NMR (Figure 6b).

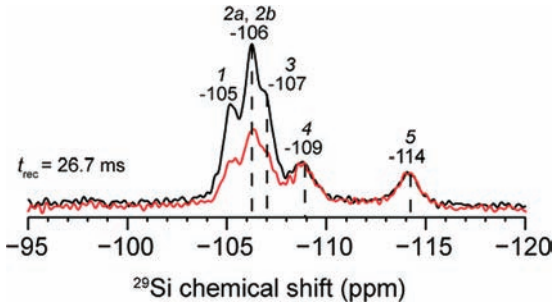

Figure 8. Superimposed solid-state 1D ^{29}Si{^{19}F} REDOR NMR spectra of as-synthesized zeolite ITW acquired at room temperature and 15 kHz MAS, using a 300 s recycle delay without (S_0, black) and with (S, red) reintroduction of ^{19}F—^{29}Si dipolar couplings during a recoupling time, t_{rec}, of 26.7 ms.

The incorporation of ^{19}F$^-$ ions within as-synthesized zeolite ITW suggests that fluoride species may also play a structure-directing role during zeolite formation, in addition to acting as a mineralizing agent and/or catalyst for Si—O—Si bond formation. Molecular interactions between ^{29}Si framework species and ^{19}F$^-$ anions can similarly be established by exploiting ^{29}Si and ^{19}F dipole—dipole interactions that influence signal intensities in 1D ^{29}Si{^{19}F} REDOR NMR spectra. Although such dipolar couplings are typically removed by rapid sample rotation at the magic angle (54.74°), they can be reintroduced during a recoupling time, t_{rec}, in ^{29}Si{^{19}F} REDOR experiments (Figure 4a) to probe the relative proximities and interactions between ^{19}F ions and the different ^{29}Si framework moieties. For example, Figure 8 shows superimposed 1D ^{29}Si{^{19}F} REDOR spectra of as-synthesized zeolite ITW acquired without (black) or with (red) reintroduction of ^{19}F—^{29}Si dipole—dipole couplings. The black spectrum was acquired with ^{19}F—^{29}Si dipole—dipole couplings averaged away during a delay of 26.7 ms in which no recoupling pulses were applied. The black REDOR spectrum is similar to the quantitative single-pulse ^{29}Si MAS spectrum in Figure 5a, except for a modest and uniform reduction in ^{29}Si signal intensity due to T_1 relaxation during the time delay (which was chosen to be the same as used in the recoupled spectrum, Figure 8, red; see Experimental Methods). Both the ^{29}Si{^{19}F} REDOR (Figure 8, black) and the single-pulse ^{29}Si NMR spectra (Figure 5a) yield the same relative integrated signal intensities (1:2:1:1:1 for ^{29}Si sites "1", "2a" and "2b", "3", "4", and "5", respectively), indicating that all of the framework ^{29}Si moieties have similar T_1 relaxation times in as-synthesized zeolite ITW.

In contrast, the red 1D ^{29}Si{^{19}F} REDOR spectrum in Figure 8 was acquired under conditions that were identical to the black spectrum, except for the application of pulses that reintroduced ^{19}F—^{29}Si dipole—dipole couplings during the 26.7 ms recoupling time. Comparison of the averaged (black) and dipolar-recoupled

(red) $^{29}Si\{^{19}F\}$ REDOR spectra in Figure 8 shows substantial ^{29}Si signal attenuation in the red spectrum, due to ^{29}Si magnetization transfer to dipole−dipole-coupled ^{19}F species. Importantly, the attenuation is nonuniform among the different ^{29}Si signals, which establishes that certain framework moieties interact more strongly with $^{19}F^-$anions than others. Specifically, the red $^{29}Si\{^{19}F\}$ REDOR spectrum exhibits clear reductions in the intensities of the ^{29}Si signals at −105, −106, and −107 ppm associated with ^{29}Si sites "1", "2a", "2b", and "3", as compared to signals at −109 and −114 ppm from ^{29}Si sites "4" and "5", for which no discernible attenuation is observed. These differences establish that the $^{19}F^-$ anions are molecularly close to and interact strongly with ^{29}Si sites "1", "2a", "2b", and "3" that form the D4R cages, and interact only weakly (if at all) with sites "4" and "5". On the basis of the ^{29}Si signal assignments determined by 2D *J*-mediated $^{29}Si\{^{29}Si\}$ DQ NMR (Figure 6a), the $^{29}Si\{^{19}F\}$ REDOR results unequivocally establish that the ^{19}F species in as-synthesized zeolite ITW are associated with the D4R cages.

Furthermore, the ^{29}Si resonances in Figure 8 corresponding to sites "1", "2a", "2b", and "3" are attenuated to the same relative extents, indicating that $^{19}F-^{29}Si$ dipole−dipole couplings between $^{19}F^-$ ions and each of the D4R-cage ^{29}Si framework sites are comparable. This suggests that the $^{19}F^-$ anions reside, on average, in the centers of the D4R cages, consistent with the D4R cages being stabilized by F^- anions as the ITW structure forms. The solid-state NMR analyses, in conjunction with XRD results, thus yield detailed new insights that provide comprehensive understanding of the interactions and relative distributions of F^- anions, organocation structure-directing molecules, and silicate framework species in as-synthesized zeolite ITW.

The structure-directing influences of the organocation SDA^+ molecules and F^- anions during synthesis of zeolite ITW are expected to be governed by the mutual interactions among the SDA^+, F^-, and silicate species as they coassemble and the framework crystallizes. The role(s) of F^- anions are manifested by the different zeolite products that result from using the same *N,N′*-2-trimethylimidazolium SDA^+ species in neutral fluoride (pH ≈ 7) versus alkaline media (pH ≈ 11): whereas zeolite ITW is formed from the solutions containing fluoride, in the absence of F^-, zeolite MTW results.[57] Zeolite MTW has a framework topology closely related to that of zeolite MTT, containing 1D 12-ring channels with no D4R cages. The different framework selectivities obtained for zeolite syntheses using *N,N′*-2-trimethylimidazolium SDA molecules with or without F^- (and accompanying solution pH differences) indicate that the fluoride species play a significant role in the formation of the zeolite ITW framework. The strong $^{19}F-^{29}Si$ dipole−dipole couplings shown to exist solely (Figure 8) between $^{19}F^-$ anions and the ^{29}Si framework atoms that form the D4R cages strongly support the hypothesis that the F^- anions promote the formation of D4R structures in the ITW framework. Furthermore, the uniform $^1H-^{29}Si$ dipole−dipole couplings between the ^1H moieties of the SDA^+ molecules and all of the ^{29}Si framework species (Figure 6b) are consistent with the importance of *N,N′*-2-trimethylimidazolium cations in directing the formation of the larger $[4^45^46^48^4]$ cages. From the mutual interactions and relative distributions of the F^- anions, SDA^+ cations, and ^{29}Si framework species established by 1D and 2D NMR, the SDA^+ and F^- ions appear to be relatively weakly associated with each other in as-synthesized zeolite ITW. As a consequence, the SDA^+ and F^- species manifest complementary structure-directing roles in the formation of the larger and smaller cages, respectively, of which the ITW framework is comprised.

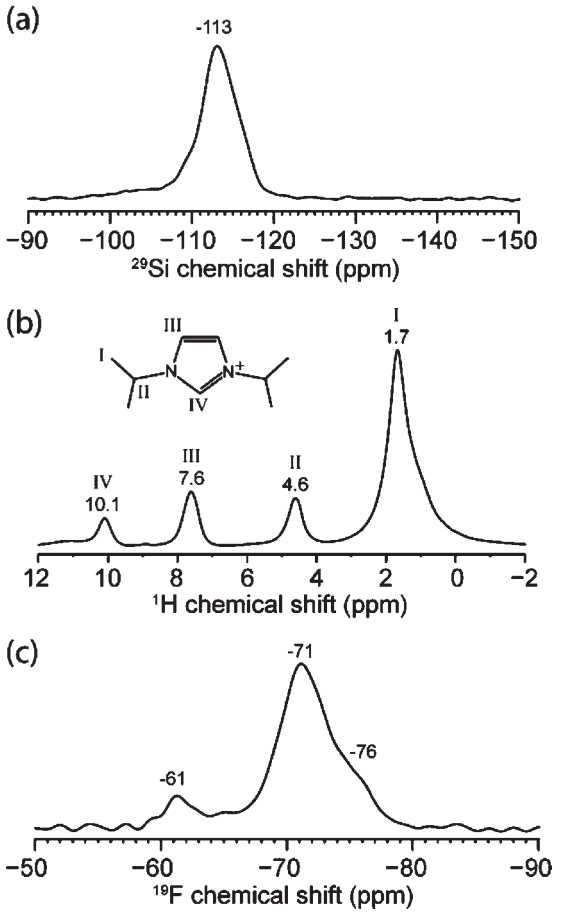

Figure 9. Solid-state 1D single-pulse (a) ^{29}Si, (b) ^1H, and (c) ^{19}F MAS NMR spectra of as-synthesized zeolite MTT acquired at room temperature under MAS conditions of 10 kHz for ^1H or 15 kHz for ^{19}F and ^{29}Si. Proton chemical shift assignments are shown in the inset in (b) for the structure-directing organocation, *N,N′*-diisopropylimidazolium.

As-Synthesized Zeolite MTT. Although synthesized under nearly identical fluoride-mediated conditions as zeolite ITW, zeolite MTT by comparison possesses an entirely different structure with no D4R cages, the reasons for which have until now remained speculative. The as-synthesized MTT framework structure is more complicated than zeolite ITW, which on the basis of previous single-crystal XRD analyses has been determined to consist of seven crystallographically distinct T-sites.[22] Of the seven T-sites, five occur four times per MTT unit cell, and the other two each occur twice, as shown in the inset of Figure 2b. Using NMR analyses similar to those for zeolite ITW above, the intermolecular interactions and distributions of F^- anions, organocation structure-directing molecules, and silicate framework species in as-synthesized zeolite MTT can be similarly probed and understood.

Despite the high extent of long-range periodic order of the MTT framework established by powder XRD (Figure 2b), the local environments of the T-sites are much more complicated. Although the MTT framework structure consists of seven crystallographically distinct T-sites, the ^{29}Si MAS NMR spectrum shown in Figure 9a of as-synthesized zeolite MTT exhibits a

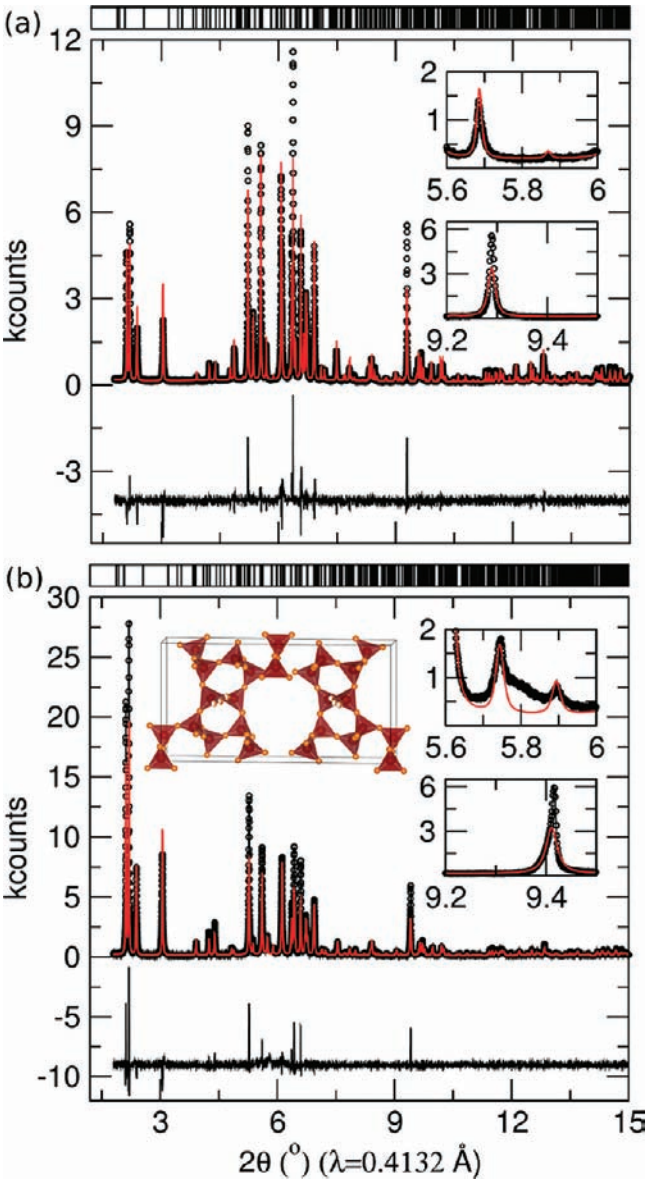

Figure 10. Synchrotron X-ray powder diffraction patterns and Rietveld refinements of (a) as-synthesized and (b) calcined zeolite MTT. The open circles correspond to experimental data, the red lines represent the Rietveld refinements using the $Pmn2_1$ space group, and the solid black lines represent the difference between simulated and experimental data. Expected reflection positions are shown on the top of both patterns. The insets in (a) and (b) are magnifications of the 2θ ranges 5.6°−6.0° (upper right) and 9.2°−9.5° (lower right), showing the comparison between the as-synthesized and calcined data in these regions. A schematic diagram of the refined calcined MTT structure looking down the *c*-axis is shown in (b), with the same atom colors as in Figure 7.

single broad (~9 ppm, fwhm) and unresolved signal centered at ca. −113 ppm, which belies the high degree of crystallinity indicated by powder XRD. By comparison, ^{29}Si MAS spectra of calcined zeolite MTT yield better resolved ^{29}Si signals corresponding to crystallographically distinct T-sites of the MTT framework (Figure S1b).[48] This indicates that the broad and poorly resolved ^{29}Si MAS spectrum (Figure 9a) of as-synthesized zeolite MTT can be attributed to subtle variations in the local environments of the different ^{29}Si T-site species. While XRD is most sensitive to scattering from the core electrons that are dependent on the positional order of atoms in the silicate frameworks, the broad distribution of isotropic ^{29}Si chemical shifts reflects nonuniform valence-electron environments.[58] Such a distribution of local electronic environments of the ^{29}Si framework sites in as-synthesized zeolite MTT, along with the narrow XRD reflections (Figure 2b), is consistent with different local configurations or distributions of the SDA^+ molecules and/or F^- species that lead accordingly to different local interactions at ^{29}Si framework sites that are otherwise molecularly ordered. Along with the predominant signal at −113 ppm, much weaker ^{29}Si intensity is observed in the region −100 to −105 ppm, which is attributed to incompletely condensed Q^3 ^{29}Si species,[54] consistent with the relatively high external surface areas of the needle-like MTT particles (Figure 3c,d). Previous 1D ^{29}Si{^{1}H} CPMAS NMR measurements of as-synthesized MTT also revealed a signal at approximately −146 ppm, indicative of five-coordinate ^{29}Si species, such as SiO_4F^- moieties.[22] However, no discernible signal intensity is observed in this region of the quantitative single-pulse ^{29}Si MAS spectrum (Figure 9a) of as-synthesized MTT, indicating that five-coordinated ^{29}Si moieties are not present in appreciable concentrations in the sample under consideration here. (Residual excess silicon fluoride species remained in solution or were washed away, as confirmed by the absence of ^{29}Si signals in the range −140 to −170 ppm that are associated with five- and six-coordinate ^{29}Si species.) In contrast to as-synthesized zeolite ITW, ^{29}Si MAS NMR thus suggests that framework ^{29}Si species in as-synthesized zeolite MTT experience distributions of interactions with the organocation structure-directing molecules and/or F^-anions, consistent with their lower extents of long-range order as separately inferred from XRD.

Synchrotron X-ray diffraction analyses of as-synthesized and calcined zeolite MTT are similarly more complicated than for zeolite ITW. The synchrotron XRD results are sensitive to subtleties in the structures of as-synthesized and calcined zeolite MTT that may otherwise go unnoticed when using Cu K_α radiation. The synchrotron XRD patterns of both as-synthesized and calcined zeolite MTT can be modeled with the orthorhombic $Pmn2_1$ space group, consistent with previous single-crystal studies of as-synthesized MTT.[22] (Rietveld refinement of the XRD data for calcined zeolite MTT using a structural model with $P12_11$ symmetry, as suggested by an earlier study of calcined NH_4F-loaded MTT,[59] does not account for several features that were modeled by the $Pmn2_1$ space group, although it led to a slightly improved overall fit (χ^2 = 3.749 for $P12_11$, χ^2 = 4.612 for $Pmn2_1$) of the reflections captured. Such improvement of the fit is likely due to the nearly 2 times larger number of crystallographically distinct atom sites in the $P12_11$ model, as compared to $Pmn2_1$ symmetry.) The Rietveld refinements of both sets of MTT data, shown in Figure 10a,b for the as-synthesized (χ^2 = 3.548) and calcined (χ^2 = 4.612) materials, respectively, are not as well fit as the $P2_1/m$ refinement of calcined zeolite ITW (χ^2 = 1.645), based on their respective χ^2 values. The poorer fits are consistent with the solid-state ^{29}Si MAS NMR results for the different zeolites, notably the as-synthesized materials (Figures 5a, 9a), which show distinct ^{29}Si peaks for zeolite ITW and a broad unresolved ^{29}Si line shape for zeolite MTT. Such a variety of local environments in zeolite MTT manifests itself in the synchrotron XRD data as relatively broad features that are difficult to model using a symmetric, periodic model. One example is shown in the upper inset of Figure 10b,

which shows reflections near 5.8° 2θ that are not accounted for by the $Pmn2_1$ space-group model of the calcined MTT structure. This region is broad, of low intensity (under 1000 counts), and is bordered by the reflections from the (301) and (510) planes at 5.7° and 5.9° 2θ, respectively. The characteristic sawtooth shape of this reflection suggests potentially some turbostratic disorder or stacking faults in the calcined MTT sample. Stacking faults are ubiquitous in the crystallography of many zeolites.[60] Upon calcination, the MTT unit cell parameters become smaller, with the loss of the organocations and F^- anions, as well as possibly increased condensation of the siliceous framework. The lower inset in Figure 10b shows the reflection from the (002) plane near 9.4° 2θ, which appears at a larger 2θ value as compared to the as-synthesized material (Figure 10a), consistent with the smaller unit cell of the calcined zeolite MTT. The synchrotron XRD analyses thus complement the ^{29}Si NMR results, corroborating that calcined zeolite MTT exhibits a lower degree of both short- and long-range order than calcined zeolite ITW.

Similarly, as-synthesized zeolite MTT exhibits more structural disorder than as-synthesized ITW and calcined MTT, as evidenced by both synchrotron XRD and ^{29}Si NMR results. Rietveld refinement of the synchrotron XRD data in Figure 10a yields atomic displacement parameters (U_i/U_e) that are an order of magnitude larger for as-synthesized zeolite MTT than for the calcined material (Supporting Information, Tables S3, S4). This indicates larger extents of disorder and/or thermal motions in the as-synthesized material. The reflection positions and intensities of the synchrotron XRD pattern in Figure 10a obtained for a bulk powder sample of as-synthesized zeolite MTT reflect the same $Pmn2_1$ symmetry as determined by an earlier single-crystal XRD study of as-synthesized zeolite MTT,[22] although with minor differences in the unit cell parameters and atomic positions (possibly due to subtle differences in the synthesis conditions of the samples). For example, refinement of the synchrotron XRD data using the $Pmn2_1$ structure reveals that the atomic displacement parameters are significantly larger for the SDA^+ and F^- species, possibly due to their greater thermal, conformational, or distributional disorder within the channels, as compared to the Si and O framework atoms. Interestingly, the synchrotron XRD pattern of as-synthesized zeolite MTT does not show the same broad reflection around 5.8° 2θ (Figure 10a) as in the calcined material (Figure 10b), and consequently the entire pattern can be fit well by the $Pmn2_1$ structural model. The reflection near 9.3° 2θ (Figure 10a), corresponding to the (002) plane, is not skewed as observed for the calcined material and is at a smaller 2θ value, reflecting the larger unit cell of as-synthesized zeolite MTT. While the determination of an accurate structure for as-synthesized zeolite MTT is thus challenged by long-range disorder of SDA^+ and fluoride species within the as-synthesized material, its siliceous framework clearly manifests a high degree of crystallinity, as evidenced by the synchrotron XRD analyses.

Nevertheless, despite their lack of long-range positional registry, the *N,N′*-diisopropylimidazolium SDA^+ molecules in as-synthesized zeolite MTT still appear to occupy relatively uniform local environments. The single-pulse ^{1}H MAS NMR spectrum shown in Figure 9b of as-synthesized MTT reveals four well-resolved ^{1}H signals centered at 1.7, 4.6, 7.6, and 10.1 ppm (labeled "I", "II", "III", and "IV", respectively). These are assigned to the four distinct ^{1}H moieties of the *N,N′*-diisopropylimidazolium structure-directing species: the methyl (I) and methine protons (II) of the isopropyl chains, ring protons (III) at the 4 and 5 positions, and ring protons (IV) at the 2 position of

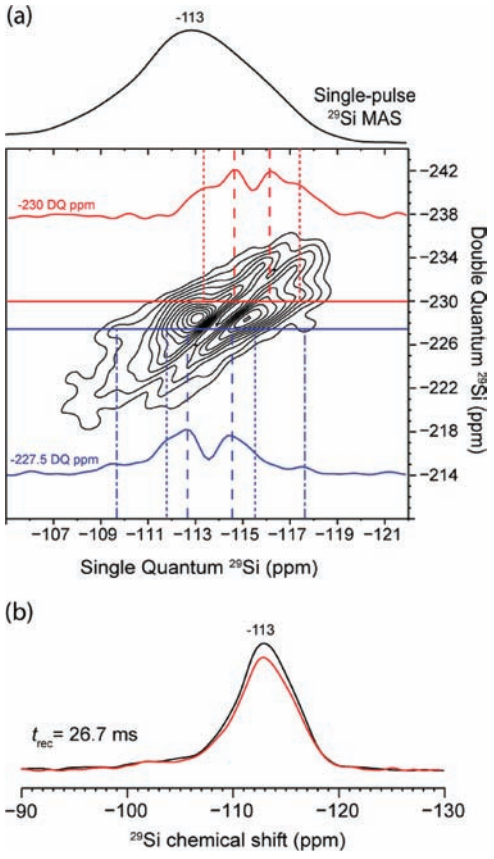

Figure 11. (a) Solid-state 2D refocused INADEQUATE (*J*-mediated) ^{29}Si{^{29}Si} DQ NMR spectrum of as-synthesized zeolite MTT acquired at room temperature and 10 kHz MAS with a single-pulse 1D ^{29}Si MAS spectrum (black) shown along the top horizontal axis. Contour slices taken at −227.5 ppm (blue) and −230 ppm (red) in the DQ dimension are shown along with partially resolved correlated signal pairs, indicated by dotted and dashed lines. (b) Superimposed solid-state 1D ^{29}Si{^{19}F} REDOR spectra of the same as-synthesized zeolite MTT sample acquired at room temperature and 15 kHz MAS, using a 300 s recycle delay without (S_0, black) and with (S, red) reintroduction of ^{19}F−^{29}Si dipolar couplings during a recoupling time t_{rec} of 26.7 ms.

the imidazolium ring. The relatively narrow (∼0.5 ppm, fwhm) ^{1}H lineshapes indicate that the SDA^+ molecules reside in uniform local environments, attributed to rapid (<1 ms) motions of the SDA^+ molecules that average ^{1}H−^{1}H dipolar couplings, as was similarly observed for as-synthesized zeolite ITW (Figure 5b). These results are consistent with the *N,N′*-diisopropylimidazolium organocations residing in the large one-dimensional 10-ring channels that permeate the MTT framework.

Whereas the single-crystal XRD analyses point to a single location for F^- anions,[22] ^{19}F MAS NMR reveals evidence of numerous $^{19}F^-$ species, including less ordered moieties that are not easily characterized by XRD. For example, the quantitative solid-state single-pulse ^{19}F MAS spectrum in Figure 9c reveals three partially resolved ^{19}F signals: two overlapping resonances at −71 and −76 ppm and a well resolved, but less intense, signal at −61 ppm. Single-crystal X-ray scattering analyses of as-synthesized MTT established the presence of only one type of ordered fluorine moieties that was attributed to a fifth ligand at a Si T-site in the five-rings of the [$5^2$6^2] cages of the MTT framework (Figure 2b, inset, light blue); 25% of such sites were estimated to be occupied by a F atom.[22] F^- moieties within

similar cages in other fluoride-containing siliceous zeolites have been shown to yield a single ^{19}F signal in the range of ca. −60 to −75 ppm,[9] leaving at least two of the three resonances observed by ^{19}F MAS NMR unaccounted for. On the basis of previous ^{19}F NMR investigations, Camblor and co-workers suggested that ^{19}F resonances in the range of −54 to −75 ppm may arise from $^{19}F^-$ anions within $[4^35^4]$ or similar cages,[9] although these are not present in the MTT framework structure. Consequently, the different F^- anion environments cannot be identified solely on the basis of single-pulse ^{19}F MAS NMR and available crystallographic analyses. Furthermore, the distributions of such ^{19}F species likely contribute to the distribution of local T-site environments that result in the broad and overlapping ^{29}Si signals (Figure 9a) from the crystallographically distinct silicate framework sites.

Although the seven crystallographically distinct T-sites in as-synthesized zeolite MTT are not resolved in 1D ^{29}Si MAS spectra, 2D NMR measurements provide enhanced spectral resolution that reveals clear evidence of short-range valence-electron ordering of the ^{29}Si framework species. Such ordering is established by careful scrutiny of the correlated signal intensities of the 2D *J*-mediated $^{29}Si\{^{29}Si\}$ DQ NMR spectrum in Figure 11a, which manifests ordered $^{29}Si-O-^{29}Si$ site pairs, even though individual correlated 2D signal intensities are not well resolved. For example, correlated signal pairs are apparent in horizontal slices taken at −227.5 ppm (blue) and −230 ppm (red) in the double-quantum dimension. Specifically, the DQ slice at −227.5 ppm reveals three partially resolved pairs of ^{29}Si signals at ca. −110 ppm/−117 ppm, ca. −112 ppm/−116 ppm, and ca. −113 ppm/−115 ppm in the SQ dimension, each corresponding to a distinct *J*-coupled $^{29}Si-O-^{29}Si$ spin pair. Similarly, the DQ slice at −230 ppm reveals two partially resolved ^{29}Si signal pairs at ca. −113 ppm/−117 ppm and ca. −114 ppm/−116 ppm in the SQ dimension that reflect interconnectivities between two additional $^{29}Si-O-^{29}Si$ pairs of sites in the MTT framework. Although the extent of ^{29}Si signal overlap precludes assignments of the correlated 2D *J*-mediated $^{29}Si\{^{29}Si\}$ NMR signals to specific framework T-site pairs, short-range ordering of the ^{29}Si framework T-sites is clearly evident in as-synthesized zeolite MTT, albeit less so than for as-synthesized zeolite ITW.

In addition, whereas certain Si framework sites (namely those in the D4R cages) in as-synthesized zeolite ITW exhibit strong and selective interactions with F^- ions, the Si T-sites in as-synthesized zeolite MTT experience uniformly weak interactions with the multiple fluorine species present (Figure 9c). This is evident in 1D $^{29}Si\{^{19}F\}$ REDOR NMR spectra, which are sensitive to interactions between $^{19}F^-$ anions and ^{29}Si moieties in the MTT framework, providing insights on their mutual local environments. As shown in Figure 11b, 1D $^{29}Si\{^{19}F\}$ REDOR spectra of as-synthesized zeolite MTT were acquired without and with (black and red, respectively) reintroduction of $^{19}F-^{29}Si$ dipole−dipole couplings, using the same 26.7 ms recoupling time as for the REDOR spectra (Figure 8) of as-synthesized zeolite ITW. Comparison of the averaged (black) and dipole-recoupled (red) $^{29}Si\{^{19}F\}$ REDOR spectra in Figure 11b reveals minor and uniform loss of ^{29}Si signal intensity across the entire range over which signals are detected from −108 to −117 ppm. As $^{19}F-^{29}Si$ dipole couplings are related to the mobilities and distances separating ^{19}F and ^{29}Si species, the small and uniform reduction in ^{29}Si REDOR signal intensity establishes that the ^{19}F species in as-synthesized zeolite MTT interact weakly and similarly with the various ^{29}Si framework species over the time scale t_{rec} = 26.7 ms. This is consistent with the $^{19}F^-$ anions being relatively mobile and, on average, approximately equidistant from all of the ^{29}Si T-sites of the MTT framework. Furthermore, taking into consideration Coulombic interactions between $^{19}F^-$ anions and SDA^+ cations, such weak $^{19}F-^{29}Si$ dipolar couplings are consistent with the majority of the $^{19}F^-$ anions in as-synthesized MTT acting as part of ion pairs with the SDA^+ molecules within the large 10-ring channels. This is in contrast to as-synthesized zeolite ITW, where the F^- and SDA^+ ions are established to reside in separate D4R and $[4^45^46^48^4]$ cages, respectively.

Consequently, differences in the interactions between the F^- anions, SDA^+ organocations, and silicate frameworks greatly influence the structure-directing roles of the F^- and SDA^+ ions and the formation of resulting zeolites ITW and MTT. Whereas F^- anions are shown to have a prominent influence on the ITW framework, zeolite MTT appears to be less affected by the presence of fluoride ions. This is further supported by the formation of zeolite MTT in syntheses using the same *N*,*N*′-diisopropylimidazolium SDA^+ molecules independent of whether alkaline or neutral fluoride media are used.[57,61] The varying roles of fluoride may be attributed to differences in the molecular interactions between the F^- anions and the respective SDA^+ molecules *N*,*N*′-2-trimethylimidazolium and *N*,*N*′-diisopropylimidazolium. F^- anions that are shown to be strongly associated with the silicate frameworks, like those in as-synthesized zeolite ITW, appear to have weaker interactions with the *N*,*N*′-2-trimethylimidazolium cations, so that both can exert distinct structure-directing influences on the crystallizing ITW framework. By comparison, for as-synthesized zeolite MTT, weak interactions between the F^- anions and the silicate framework indicate that the F^- and *N*,*N*′-diisopropylimidazolium species form ion pairs. As a result, the F^- anions do not manifest distinct structure-directing effects on the crystalline MTT framework, consistent with the absence of D4R cages in the $Pmn2_1$ MTT structure. Rather, F^- anions likely function principally as mineralizing agents during syntheses of zeolite MTT. Further investigations of transient interactions of these different species and their consequences on the crystallization of zeolite and silicate frameworks are currently underway in our laboratories.

■ CONCLUSIONS

The molecular interactions and proximities of F^- ions, SDA^+ molecules, and siliceous zeolite frameworks are established and shown to differ significantly in as-synthesized zeolites ITW and MTT. Solid-state 1D and 2D NMR measurements of through-bond *J*- and through-space dipolar couplings provide new molecular insights on $^{29}Si-O-^{29}Si$ connectivities between framework T-sites and their interactions with the SDA^+ and F^- ions. This includes SDA^+ and F^- species in environments that lack long-range order. Using 2D $^{29}Si\{^{29}Si\}$ *J*-mediated (refocused INADEQUATE) and 1D $^{29}Si\{^{19}F\}$ REDOR NMR, F^- anions were determined to reside in D4R cages in zeolite ITW and interact strongly with the silicate framework, imparting a structure-directing influence that is distinct from the SDA^+ molecules. In addition, the ITW framework was shown to have a lower symmetry than previously reported, with the structure of calcined zeolite ITW falling under the $P2_1/m$ space group. The determination of the $P2_1/m$ framework symmetry was enabled by advanced 2D NMR methods, which in conjunction with synchrotron X-ray scattering

analyses allow for more accurate determination of structures in materials with complicated combinations of long- and short-range order and disorder.

Both zeolites ITW and MTT were found to have lower symmetry or less ordered structures in the as-synthesized, as compared to the calcined, materials. Calcined zeolite ITW was modeled well by the $P2_1/m$ structure and as-synthesized ITW by the $P2_1$ structure. Structures of both MTT materials can be refined successfully with the previously proposed $Pmn2_1$ structure. In contrast to zeolite ITW, F^- anions in as-synthesized zeolite MTT were determined to reside predominantly with the *N,N′*-diisopropylimidazolium SDA^+ molecules as ion pairs in the 10-ring channels of the MTT framework. The stark differences in F^- ion environments associated with as-synthesized zeolites ITW and MTT are perhaps unexpected, given the similarities in their respective alkyl-imidazolium SDAs and otherwise identical synthesis conditions. Such differences in F^- interactions and the resulting structural differences in the ITW and MTT topologies are attributed to subtle differences in the architectures of similar SDA^+ molecules, which determine whether F^- anions exert distinct influences on the crystallizing silicate frameworks or do so as part of F^-—SDA^+ ion pairs. In both cases, intermolecular interactions among the F^-, SDA^+, and silicate species play crucial roles in the nucleation and development of framework ordering in zeolites. Such molecular-level understanding of the local environments of the F^- and SDA^+ ions and their interactions with crystalline zeolite frameworks are expected to aid generally the design of structure-directing species and conditions that can enable the control of how different crystal structures develop and the topologies that result.

■ ASSOCIATED CONTENT

Supporting Information. Atomic positions, displacement factors, and unit cell parameters for Rietveld-refined as-synthesized and calcined zeolite ITW and MTT structures; and solid-state 1D single-pulse ^{29}Si MAS NMR spectra of calcined zeolites ITW and MTT. This material is available free of charge via the Internet at http://pubs.acs.org.

■ AUTHOR INFORMATION

Corresponding Author
bradc@engineering.ucsb.edu

Present Address
[#]Exxonmobil, 1545 Route 22 East, Annandale, NJ 08801

■ ACKNOWLEDGMENT

We thank Dr. S. Cadars, M. F. Hsieh, and J. Kurzman for helpful discussions. This work was supported in part by the U.S. Department of Energy, Basic Energy Sciences, Catalysis Science Grant no. DE-FG02-03ER15467, the National Science Foundation, Grant no. CHE-0924654, the ConvEne IGERT Program (NSF-DGE 0801627), and by Chevron Energy Technology Co. (Richmond, CA). The XRD and NMR measurements made use of the Central Facilities of the UCSB Materials Research Laboratory supported by the MRSEC Program of the NSF under award no. DMR 05-20415. Use of the Advanced Photon Source (11-BM) was supported by the U.S. Department of Energy, Office of Science, Office of Basic Energy Sciences, under contract no. DE-AC02-06CH11357.

■ REFERENCES

(1) Flanigen, E. M.; Patton, R. L. Silica Polymorph and Process for Preparing Same. U.S. Patent 4,073,865, 1978.
(2) Delmotte, L.; Soulard, M.; Guth, F.; Seive, A.; Lopez, A.; Guth, J. L. *Zeolites* **1990**, *10*, 778–783.
(3) Estermann, M.; McCusker, L. B.; Baerlocher, C.; Merrouche, A.; Kessler, H. *Nature* **1991**, *352*, 320–323.
(4) Axon, S. A.; Klinowski, J. *Appl. Catal., A* **1992**, *81*, 27–34.
(5) Kuperman, A.; Nadimi, S.; Oliver, S.; Ozin, G. A.; Garces, J. M.; Olken, M. M. *Nature* **1993**, *365*, 239–242.
(6) Camblor, M. A.; Corma, A.; Valencia, S. *Chem. Commun.* **1996**, 2365–2366.
(7) Camblor, M. A.; Villaescusa, L. A.; Diaz-Cabanas, M. J. *Top. Catal.* **1999**, *9*, 59–76.
(8) Villaescusa, L. A.; Barrett, P. A.; Camblor, M. A. *Angew. Chem., Int. Ed.* **1999**, *38*, 1997–2000.
(9) Camblor, M. A.; Barrett, P. A.; Diaz-Cabanas, M. J.; Villaescusa, L. A.; Puche, M.; Boix, T.; Perez, E.; Koller, H. *Microporous Mesoporous Mater.* **2001**, *48*, 11–22.
(10) Auerbach, S. M.; Carrado, K. A.; Dutta, P. K. *Handbook of Zeolite Science and Technology*; Taylor and Francis, Inc.: New York, 2003.
(11) Barrett, P. A.; Camblor, M. A.; Corma, A.; Jones, R. H.; Villaescusa, L. A. *J. Phys. Chem. B* **1998**, *102*, 4147–4155.
(12) Blasco, T.; Camblor, M. A.; Corma, A.; Esteve, P.; Guil, J. M.; Martinez, A.; Perdigon-Melon, J. A.; Valencia, S. *J. Phys. Chem. B* **1998**, *102*, 75–88.
(13) Koller, H.; Wolker, A.; Villaescusa, L. A.; Diaz-Cabanas, M. J.; Valencia, S.; Camblor, M. A. *J. Am. Chem. Soc.* **1999**, *121*, 3368–3376.
(14) Fyfe, C. A.; Brouwer, D. H.; Lewis, A. R.; Villaescusa, L. A.; Morris, R. E. *J. Am. Chem. Soc.* **2002**, *124*, 7770–7778.
(15) Darton, R. J.; Brouwer, D. H.; Fyfe, C. A.; Villaescusa, L. A.; Morris, R. E. *Chem. Mater.* **2004**, *16*, 600–603.
(16) Zicovich-Wilson, C. M.; Gándara, F.; Monge, A.; Camblor, M. A. *J. Am. Chem. Soc.* **2010**, *132*, 3461–3471.
(17) Attfield, M. P.; Catlow, C. R. A.; Sokol, A. A. *Chem. Mater.* **2001**, *13*, 4708–4713.
(18) Caullet, P.; Paillaud, J. L.; Simon-Masseron, A.; Soulard, M.; Patarin, J. *C. R. Chim.* **2005**, *8*, 245–266.
(19) Barrett, P. A.; Diaz-Cabanas, M. J.; Camblor, M. A.; Jones, R. H. *J. Chem. Soc., Faraday Trans.* **1998**, *94*, 2475–2481.
(20) Camblor, M. A.; Diaz-Cabanas, M.-J.; Perez-Pariente, J.; Teat, S. J.; Clegg, W.; Shannon, I. J.; Lightfoot, P.; Wright, P. A.; Morris, R. E. *Angew. Chem., Int. Ed.* **1998**, *37*, 2122–2126.
(21) Barrett, P. A.; Boix, T.; Puche, M.; Olson, D. H.; Jordan, E.; Koller, H.; Camblor, M. A. *Chem. Commun.* **2003**, 2114–2115.
(22) Zones, S. I.; Darton, R. J.; Morris, R.; Hwang, S. J. *J. Phys. Chem. B* **2005**, *109*, 652–661.
(23) Burton, A. W. *J. Am. Chem. Soc.* **2007**, *129*, 7627–7637.
(24) Koller, H.; Wölker, A.; Eckert, H.; Panz, C.; Behrens, P. *Angew. Chem., Int. Ed. Engl.* **1997**, *36*, 2823–2825.
(25) Fyfe, C. A.; Lewis, A. R.; Chezeau, J. M.; Grondey, H. *J. Am. Chem. Soc.* **1997**, *119*, 12210–12222.
(26) Fyfe, C. A.; Brouwer, D. H.; Lewis, A. R.; Chezeau, J. M. *J. Am. Chem. Soc.* **2001**, *123*, 6882–6891.
(27) Pulido, A.; Corma, A.; Sastre, G. *J. Phys. Chem. B* **2006**, *110*, 23951–23961.
(28) George, A. R.; Catlow, C. R. A. *Zeolites* **1997**, *18*, 67–70.
(29) Sastre, G.; Gale, J. D. *Chem. Mater.* **2005**, *17*, 730–740.
(30) Price, G. D.; Pluth, J. J.; Smith, J. V.; Bennett, J. M.; Patton, R. L. *J. Am. Chem. Soc.* **1982**, *104*, 5971–5977.
(31) Caullet, P.; Guth, J. L.; Hazm, J.; Lamblin, J. M.; Gies, H. *Eur. J. Solid State Inorg. Chem.* **1991**, *28*, 345–361.
(32) van de Goor, G.; Freyhardt, C. C.; Behrens, P. *Z. Anorg. Allg. Chem.* **1995**, *621*, 311–322.

(33) Bull, L. M.; Bussemer, B.; Anupold, T.; Reinhold, A.; Samoson, A.; Sauer, J.; Cheetham, A. K.; Dupree, R. *J. Am. Chem. Soc.* **2000**, *122*, 4948–4958.
(34) Zones, S. I. Molecular Sieves Using an Imidazole Template. U.S. Patent 4,483,835, 1984.
(35) www.iza-online.org.
(36) Yang, X. B.; Camblor, M. A.; Lee, Y.; Liu, H. M.; Olson, D. H. *J. Am. Chem. Soc.* **2004**, *126*, 10403–10409.
(37) Rohrman, A. C., Jr.; LaPierre, R. B.; Schlenker, J. L.; Wood, J. D.; Valyocsik, E. W.; Rubin, M. K.; Higgins, J. B.; Rohrbaugh, W. J. *Zeolites* **1985**, *5*, 352–354.
(38) Wang, J.; Toby, B. H.; Lee, P. L.; Ribaud, L.; Antao, S. M.; Kurtz, C.; Ramanathan, M.; Von, D. R. B.; Beno, M. A. *Rev. Sci. Instrum.* **2008**, *79*, 085105/1–085105/7.
(39) Lee, P. L.; Shu, D.; Ramanathan, M.; Preissner, C.; Wang, J.; Beno, M. A.; Von Dreele, R. B.; Ribaud, L.; Kurtz, C.; Antao, S. M.; Jiao, X.; Toby, B. H. *J. Synchrotron Radiat.* **2008**, *15*, 427–432.
(40) Toby, B. H.; Huang, Y.; Dohan, D.; Carroll, D.; Jiao, X. S.; Ribaud, L.; Doebbler, J. A.; Suchomel, M. R.; Wang, J.; Preissner, C.; Kline, D.; Mooney, T. M. *J. Appl. Crystallogr.* **2009**, *42*, 990–993.
(41) Dalesio, L. R.; Hill, J. O.; Kraimer, M.; Lewis, S.; Murray, D.; Hunt, S.; Watson, W.; Clausen, M.; Dalesio, J. *Nucl. Instrum. Methods Phys. Res., Sect. A* **1994**, *352*, 179–184.
(42) Boultif, A.; Louer, D. *J. Appl. Crystallogr.* **2004**, *37*, 724–731.
(43) Larson, A. C.; Dreele, R. B. V. "General Structure Analysis System (GSAS)", Los Alamos National Laboratory Report LAUR 86-748, 2000.
(44) Toby, B. H. *J. Appl. Crystallogr.* **2001**, *34*, 210–213.
(45) Momma, K.; Izumi, F. *J. Appl. Crystallogr.* **2008**, *41*, 653–658.
(46) Gullion, T.; Schaefer, J. *J. Magn. Reson.* **1989**, *81*, 196–200.
(47) Fyfe, C. A.; Feng, Y.; Gies, H.; Grondey, H.; Kokotailo, G. T. *J. Am. Chem. Soc.* **1990**, *112*, 3264–3270.
(48) Fyfe, C. A.; Grondey, H.; Feng, Y.; Kokotailo, G. T.; Ernst, S.; Weitkamp, J. *Zeolites* **1992**, *12*, 50–53.
(49) Morris, R. E.; Weigel, S. J.; Henson, N. J.; Bull, L. M.; Janicke, M. T.; Chmelka, B. F.; Cheetham, A. K. *J. Am. Chem. Soc.* **1994**, *116*, 11849–11855.
(50) Lesage, A.; Bardet, M.; Emsley, L. *J. Am. Chem. Soc.* **1999**, *121*, 10987–10993.
(51) Fayon, F.; Massiot, D.; Levitt, M. H.; Titman, J.; Gregory, D. H.; Duma, L.; Emsley, L.; Brown, S. P. *J. Chem. Phys.* **2005**, *122*, 194313/1–194313/14.
(52) Cadars, S.; Julien, S.; Duma, L.; Lesage, A.; Pham, T. N.; Baltisberger, J. H.; Brown, S. P.; Emsley, L. *J. Magn. Reson.* **2007**, *188*, 24–34.
(53) Cadars, S.; Brouwer, D. H.; Chmelka, B. F. *Phys. Chem. Chem. Phys.* **2009**, *11*, 1825–1837.
(54) Engelhardt, G.; Michel, D. *High-Resolution Solid-State NMR of Silicates and Zeolites*; Wiley: New York, 1987.
(55) Villaescusa, L. A.; Barrett, P. A.; Camblor, M. A. *Chem. Mater.* **1998**, *10*, 3966–3973.
(56) Hedin, N.; Graf, R.; Christiansen, S. C.; Gervais, C.; Hayward, R. C.; Eckert, J.; Chmelka, B. F. *J. Am. Chem. Soc.* **2004**, *126*, 9425–9432.
(57) Zones, S. I. *Zeolites* **1989**, *9*, 458–467.
(58) Cadars, S.; Smith, B. J.; Epping, J. D.; Acharya, S.; Belman, N.; Golan, Y.; Chmelka, B. F. *Phys. Rev. Lett.* **2009**, *103*, 136802/1–136802/4.
(59) Marler, B.; Deroche, C.; Gies, H.; Fyfe, C. A.; Grondey, H.; Kokotailo, G. T.; Feng, Y.; Ernst, S.; Weitkamp, J.; Cox, D. E. *J. Appl. Crystallogr.* **1993**, *26*, 636–644.
(60) Treacy, M. M. J.; Newsam, J. M.; Deem, M. W. *Proc. R. Soc. London, Ser. A* **1991**, *433*, 499–520.
(61) Archer, R. H.; Zones, S. I.; Davis, M. E. *Microporous Mesoporous Mater.* **2010**, *130*, 255–265.